ECONSTOR
Make Your Publications Visible.

A Service of

ZBW Leibniz-Informationszentrum Wirtschaft
Leibniz Information Centre for Economics

Arora, B. B.; Bhattacharjee, Sourajit; Kashyap, Vishesh; Khan, M. N.; Tlili, I.

Article

Aerodynamic effect of bicycle wheel cladding: A CFD study

Energy Reports

Provided in Cooperation with:
Elsevier

Suggested Citation: Arora, B. B.; Bhattacharjee, Sourajit; Kashyap, Vishesh; Khan, M. N.; Tlili, I. (2019) : Aerodynamic effect of bicycle wheel cladding: A CFD study, Energy Reports, ISSN 2352-4847, Elsevier, Amsterdam, Vol. 5, pp. 1626-1637, https://doi.org/10.1016/j.egyr.2019.11.014

This Version is available at:
https://hdl.handle.net/10419/243698

Standard-Nutzungsbedingungen:

Die Dokumente auf EconStor dürfen zu eigenen wissenschaftlichen Zwecken und zum Privatgebrauch gespeichert und kopiert werden.

Sie dürfen die Dokumente nicht für öffentliche oder kommerzielle Zwecke vervielfältigen, öffentlich ausstellen, öffentlich zugänglich machen, vertreiben oder anderweitig nutzen.

Sofern die Verfasser die Dokumente unter Open-Content-Lizenzen (insbesondere CC-Lizenzen) zur Verfügung gestellt haben sollten, gelten abweichend von diesen Nutzungsbedingungen die in der dort genannten Lizenz gewährten Nutzungsrechte.

Terms of use:

Documents in EconStor may be saved and copied for your personal and scholarly purposes.

You are not to copy documents for public or commercial purposes, to exhibit the documents publicly, to make them publicly available on the internet, or to distribute or otherwise use the documents in public.

If the documents have been made available under an Open Content Licence (especially Creative Commons Licences), you may exercise further usage rights as specified in the indicated licence.

https://creativecommons.org/licenses/by/4.0/

WWW.ECONSTOR.EU

Mitglied der Leibniz-Gemeinschaft

Energy Reports 5 (2019) 1626–1637

Contents lists available at ScienceDirect

Energy Reports

journal homepage: www.elsevier.com/locate/egyr

Research paper

Aerodynamic effect of bicycle wheel cladding — A CFD study

B.B. Arora [a], Sourajit Bhattacharjee [a], Vishesh Kashyap [a], M.N. Khan [b], Iskander Tlili [c,d,*]

[a] Department of Mechanical, Production & Industrial and Automobile Engineering, Delhi Technological University, Delhi, India
[b] Department of Mechanical and Industrial Engineering, College of Engineering, Majmaah University, Majmaah 11952, Saudi Arabia
[c] Department for Management of Science and Technology Development, Ton Duc Thang University, Ho Chi Minh City, Vietnam
[d] Faculty of Applied Sciences, Ton Duc Thang University, Ho Chi Minh City, Vietnam

ARTICLE INFO

Article history:
Received 10 September 2019
Received in revised form 23 October 2019
Accepted 6 November 2019
Available online xxxx

Keywords:
Sports engineering
Bicycle
CFD
Aerodynamic drag
Drag coefficient
Cladding

ABSTRACT

Aerodynamic drag in a bicycle can originate through the rotation of wheels, and the addition of cladding on the wheels has a pronounced impact on the same. In the present work, the effect of cladding on the wheels of a bicycle is studied in terms of the percentage cladding in order to predict the aerodynamic drag using a validated CFD model. SolidWorks Flow Simulation is used to conduct an external analysis of flow air around the bicycle and rider. The k-ε turbulence model is used to study aerodynamic drag among cladding percentages varying between nil to maximum, i.e., 100%. The aerodynamic drag force is observed to decrease with increase in cladding percentage. Analyses were carried out at velocities 6 m/s, 8 m/s and 10 m/s and there was an observed maximum decrease in drag coefficient in the range of 5.2–5.3% as compared to the bicycle without cladding.

© 2019 The Authors. Published by Elsevier Ltd. This is an open access article under the CC BY license (http://creativecommons.org/licenses/by/4.0/).

1. Introduction

Cyclists utilize a large amount of power to overcome the aerodynamic drag experienced by them. Aerodynamic drag may represent between 70% and 90% of the total resistance experienced by a cyclist riding a bicycle (Chowdhury et al., 2011b; Debraux et al., 2011). The power required by the cyclist to overcome this resistance is a third-order polynomial of the velocity of travel (Swain, 1994). However, the power of a cyclist may be considered limited, and as the competitiveness of sports increases, so does the need to improve the design of equipment in order to achieve better levels of performance with the same effort. Such improvements in design can be made possible by reducing the aerodynamic drag.

The rotation of wheels is a major source of drag in a bicycle. The drag created by conventional spoked wheels can be limited by reducing the number of spokes. However, strength and rigidity factors limit this ability (García-López et al., 2008; Greenwell et al., 1995). A number of studies have attempted to examine the aerodynamics of bicycle wheels, primarily through wind tunnel and field tests. Kyle and Burke (1984), Godo et al. (2009) and Wickern et al. (1997), through experimental analysis, observed a considerable difference in the aerodynamic drag observed in rotating and stationary wheels. Sunter and Sayers (2001) analyzed the differences in the aerodynamic drag and power expended by eight different wheels, and attributed these to characteristics such as the tire diameter, width and profile. Karabelas and Markatos (2012) similarly observed that the rotation of wheels significant increased the drag and side force, and that an increase in the number of spokes also increased the axial drag and vertical force on the wheel. Jermy et al. (2008) analyzed the power dissipated by aerodynamic resistance for a range of bicycle wheels, and found that rotational drag due to wheels comprised 10–15% of the drag experience by the bicycle. Zdravkovich (1992), Crane and Morton (2018), Greenwell et al. (1995) and Tew and Sayers (1999) conducted experimental studies on a range of bicycle wheels, and concluded that aerodynamically designed wheels such as tri-spoke and disk wheels exhibited a considerable reduction in aerodynamic drag, up to 50% as compared to commercially utilized wheels. It was also observed that velocity of rotation did not have a large impact on the drag coefficient of a wheel. Dyer and Noroozi (2015) conducted field tests on nine different cycle wheels and found the power expended with the traditional spoked wheel to be over 20% higher as compared to deep section wheels, whereas the full disk wheel was observed to expend the lowest power. Monte et al. (2016) observed that non-spoked continuous wheels were aerodynamically advantageous and exhibited lower drag than discontinuous and spoked wheels. Barry et al. (2012) compared the experimental results obtained for a range of wheels in a cycle-only configuration with those obtained when a rider was included in the analysis and observed a significant impact on the drag area trends, suggesting that the choice of wheels must not be based on the individual aerodynamic characteristics of the wheels alone,

* Corresponding author.
E-mail address: iskander.tlili@tdtu.edu.vn (I. Tlili).

https://doi.org/10.1016/j.egyr.2019.11.014
2352-4847/© 2019 The Authors. Published by Elsevier Ltd. This is an open access article under the CC BY license (http://creativecommons.org/licenses/by/4.0/).

but also on biomechanic characteristics concerned with the rider. Petrone et al. (2018) similarly applied a full-scale methodology in the analysis of a cyclist riding a cycle with three different sets of spoked wheels and observed a change of 3.7% to 9% in time required in competitive time trial conditions.

Computational fluid dynamics (CFD) is powerful tool the use of which has been increasing in regularity over the past decades. Increased computational power has meant that complex CFD simulations can now be conducted in formerly reclusive fields such as bioenergy (Madhania et al., 2019), microfluids (Asadollahi et al., 2018), nanofluid mechanics (Esfahani et al., 2017; Mansour and Bakier, 2015; Milani Shirvan et al., 2017a,b; Rashidi et al., 2018, 2017) and acoustics (Kashyap and Bhattacharjee, 2019). Since cycling aerodynamics involves the study of the flow of air across an external body, i.e., a bicycle, computational fluid dynamics can be used for analysis (Defraeye et al., 2010a; Kashyap and Bhattacharjee, 2019). Knupe and Farmer (2009) and Godo et al. (2010) conducted an experimental and computational analysis of the flow of air across a bicycle wheel and observed the CFD results to be in good agreement with the wind tunnel results, thus validating the use of CFD in the context. Schwab et al. (2018) used computer model analysis to study the effect of crosswinds on the dynamics and control of a bicycle, and observed that crosswinds adversely affect the stability of a bicycle and increase its tendency to steer into the wind. Blocken et al. (2013) analyzed the impact of fender coverage angle on the drag experienced by a bicycle computationally, and obtained an optimum angle for reduced drag. Yu et al. (2018) analyzed various computational methods for the study of wheel rotation, and concluded moving wall and moving reference frame methods were appropriate when aerodynamic drag was of import. Mannion et al. (2018) computationally analyzed the moving wall, moving reference frame and sliding mesh approaches in the modeling of bicycle wheel rotation, and observed results to be in good concordance with CFD values. Hobeika and Sebben (2018) concluded that the moving reference frame method was appropriate for modeling wheel rotation independent of geometry. Ilea et al. (2019) studied the impact of wheels rims on the aerodynamics of wheels, and observed that alloy rims performed better. Pogni and Petrone (2016) used CFD for the analysis of five spoked wheels using the k-ε model for a range of yaw angles, and reported results of drag and side forces, observing deeper wheel rims offered greater aerodynamic advantages.

The addition of cladding on bicycle wheels plays an important role in the reduction of aerodynamic drag force and drag coefficient (Sayers and Stanley, 1994; Zdravkovich, 1992). The same can have a substantial effect on the power expended by the cyclist. On a survey of available literature, it is observed that a computational or parametric analysis of the effect of cladding on these aerodynamic parameters of a bicycle is sparsely available. The current work is an attempt in this direction.

In the present study, analyses have been carried out in order to determine the frontal area, aerodynamic drag force and drag coefficient as a function of percentage cladding, using Computational Fluid Dynamics. The diameter of the cladding varies from 0% to 100% of wheel diameter with a difference of 10% between consecutive analyses. The impact of velocity has been studied by simulating at 6 m/s, 8 m/s and 10 m/s.

2. Methodology

For the present study, the Computer-Aided Design (CAD) modeling of the geometry was first carried out. The geometry was then meshed and grid independence tests were performed in order to ascertain the appropriate grid fineness. CFD analysis was performed on the optimized mesh and the results were validated by comparison with reported data. The validated model was then used for performing the parametric study.

2.1. CAD model

The 3-dimensional CAD assembly was modeled according to a standard city bicycle containing the following parts — the bicycle frame, wheels (2 nos., 32 spokes each), cladding (2 nos.), cyclist (a female of height 5 ft 11 in.), helmet and a solid plane under the bicycle wheels, representing the road. The cladding constitutes two disks on either side of the wheel, present on both the front and back wheel of the bicycle, and the center of the cladding disks coincides with the wheel center. The various dimensions of the bicycle and cyclist are shown in Fig. 2.1. The assembly was created using Autodesk Fusion360 and SolidWorks, as shown in Fig. 2.2.

The diameter of the cladding was varied between 0% and 100% of the diameter of the wheel, with a difference of 10% between consecutive assemblies. SolidWorks was used to compute the frontal areas of the various CAD assemblies used for the present study. Fig. 2.3 shows the frontal areas plotted as a function of the percentage cladding.

2.2. Mathematical modeling

The algorithm used for the analysis is depicted using a flow chart shown in Fig. 2.4. SolidWorks Flow Simulation was used for the CFD analysis. Flow Simulation uses a time-implicit solver for the approximation of convective/diffusive equations for low compressible flows such as those in the current study. Defraeye et al. (2010a) studied various turbulence models and concluded that the aerodynamic drag of cyclists was most accurately predicted by the k-ε model as compared to the corresponding wind tunnel result. Taking these findings as a basis, the k-ε model was used for the current study. The analysis was governed by the 3D steady Favre Averaged Navier–Stokes (FANS) (Sobachkin and Dumnov, 2013) equations solved with second-order accuracy using the k-ε model (Jones and Launder, 1973), which were then discretized over the domain using the finite-volume method. Favre-averaging is beneficial in the given physical conditions, since it simplifies the averaged equations significantly by suppressing terms related to density fluctuations in compressible flow. The finite-volume method ensures that spatial discretization is performed in the physical space, reducing the possibility of errors derived from transformation between the physical and computational coordinate system. The governing equations are as follows (Sobachkin and Dumnov, 2013).

$$\frac{\partial \rho}{\partial t} + \frac{\partial (\rho u_i)}{\partial x_i} = 0 \tag{1}$$

where the density of the medium is represented by ρ, time is represented by t and velocity of flow in the x_i direction is represented by u_i.

$$\frac{\partial (\rho u_i)}{\partial t} + \frac{\partial}{\partial x_j}\left(\rho u_i u_j\right) + \frac{\partial P}{\partial x_i} = \frac{\partial}{\partial x_j}\left(\tau_{ij} + \tau_{ij}^R\right) + S_i \tag{2}$$

where velocity in the x_j direction is represented by u_j, represents fluid pressure is represented by P, the shear stress tensor is represented by τ_{ij} and body force is represented by S_i.

A computational domain of length 32 m, height 8 m and width 8 m was chosen in accordance with best practice guidelines (Franke et al., 2007) as shown in Fig. 2.5. To simulate the travel of the bicycle on a road, the road was modeled as a non-slip moving wall with its velocity equal to the relative velocity of travel of the bicycle with respect to air. All analyses were carried out at an ambient pressure and temperature of 1 bar and 298 K respectively. Inlet velocities of 6, 8 and 10 m/s were applied as a uniform velocity profile on the upstream face of

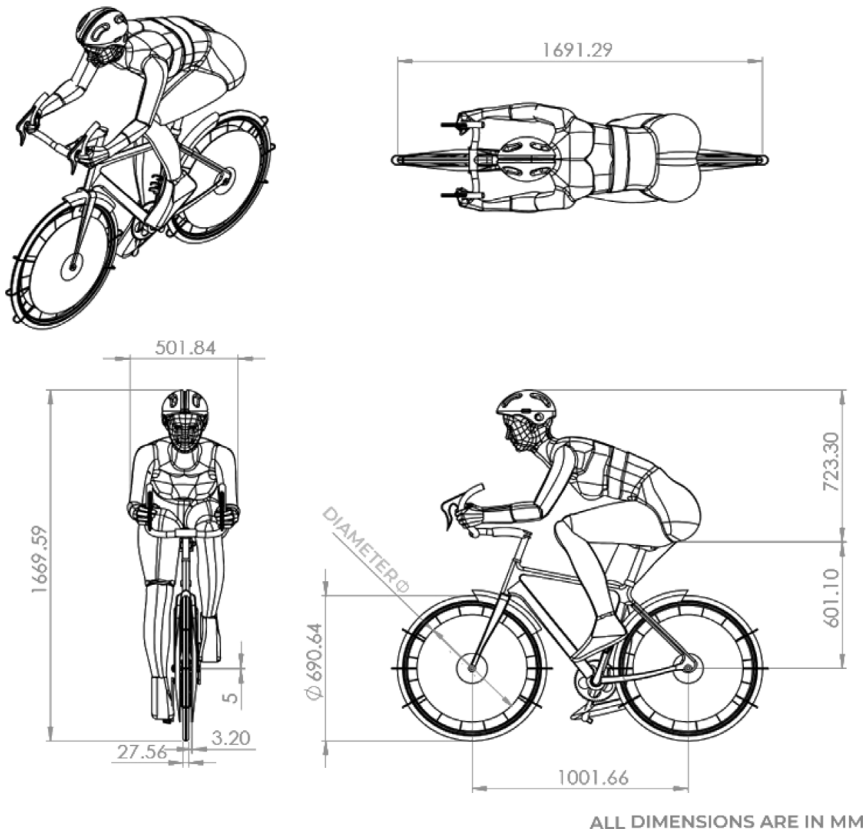

Fig. 2.1. Dimensions and geometry of bicycle and cyclist.

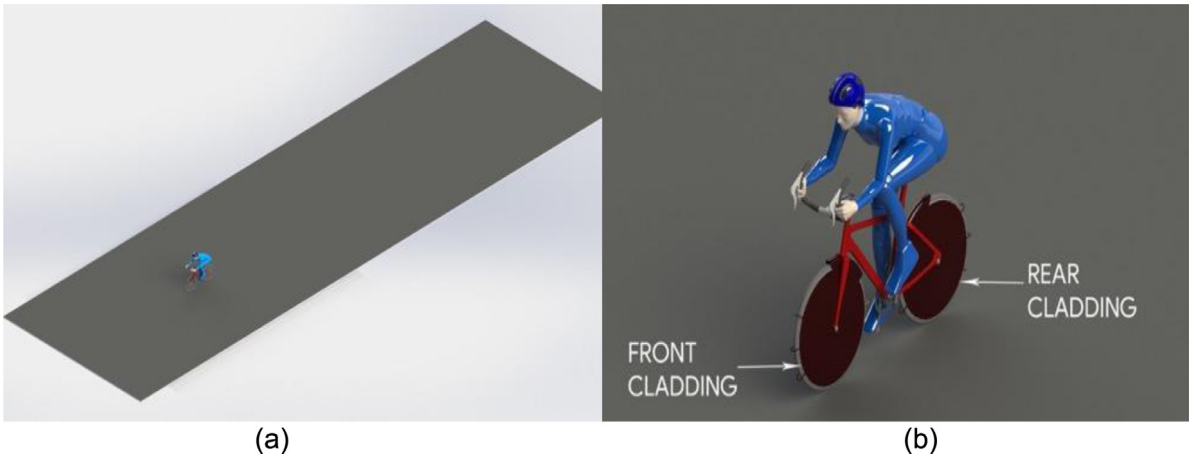

Fig. 2.2. The CAD assembly used in the analysis (a) wide isometric view (b) close-in isometric view.

the computational domain, while the downstream face was given an ambient pressure outlet. The wheels were given a rotational velocity corresponding to the relative velocity of travel. Table 2.1 lists the input and output parameters defined for the analysis.

The following equations were used to define the drag coefficient and lift coefficient.

$$C_D = F_D/\left(0.5\rho A_D v^2\right) \tag{3}$$

$$C_L = F_L/\left(0.5\rho A_L v^2\right) \tag{4}$$

The required grid fineness for the parametric study was chosen by performing a grid independence study (Arora, 2014). SolidWorks Flow Simulation implements a Cartesian meshing scheme, which carries the advantages of a robust differential scheme, minimized truncation errors and greater speed (Sobachkin and Dumnov, 2013). The fineness of the mesh is represented by the ratio factor. This ratio factor governs the relative size of the Cartesian mesh elements. A greater ratio factor represents higher fineness in the section containing the CAD model.

Further parametric study was carried out to find the effect of cladding percentage on the aerodynamic drag force and drag coefficient of a bicycle being ridden by a cyclist. The diameter of the cladding was varied between 0% and 100% of the diameter of the wheel, with a difference of 10% between consecutive analyses. The effect of velocity on the drag force and drag coefficient was also studied by varying the velocity from 6 m/s to 10 m/s. Convergence was monitored and the analysis was concluded when residuals of velocity components, continuity, k and ε reached an

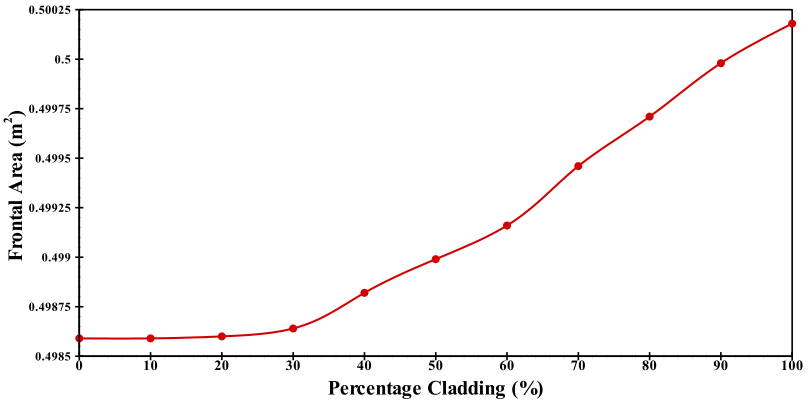

Fig. 2.3. Frontal areas of CAD models as a function of percentage cladding.

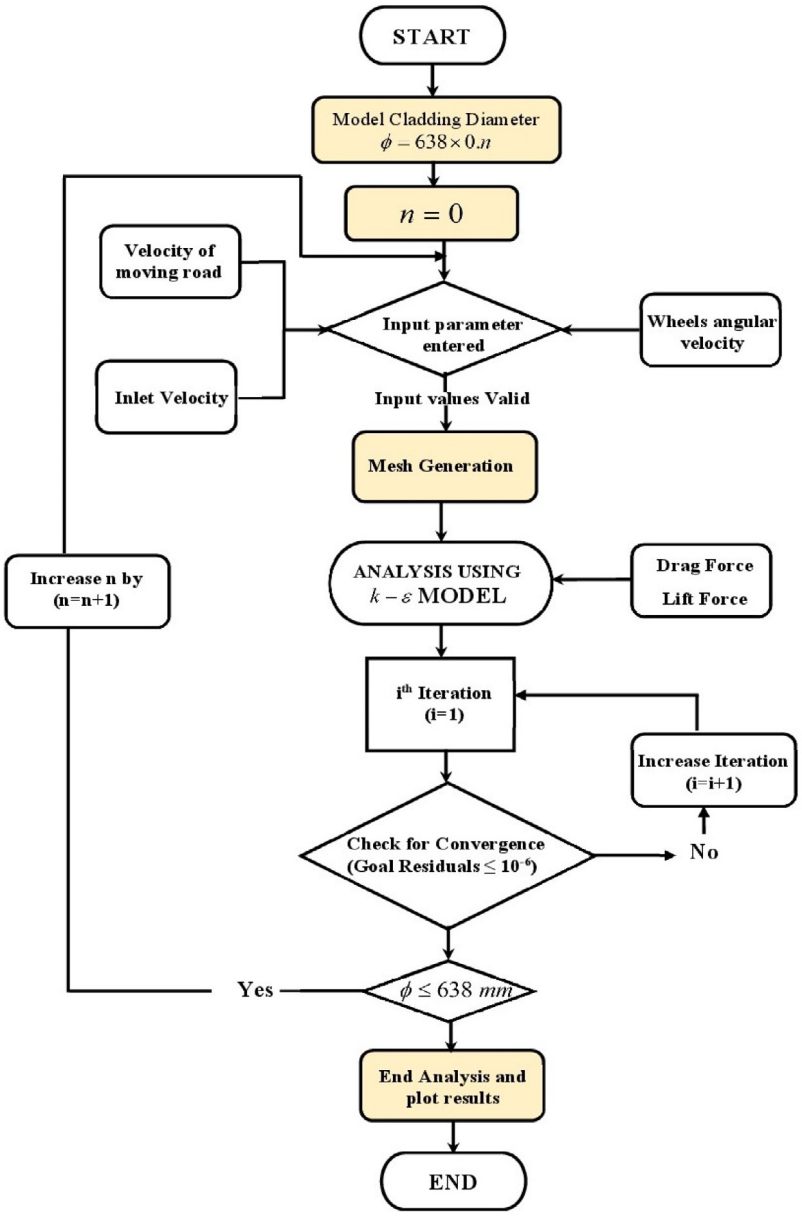

Fig. 2.4. Flow chart of analysis algorithm.

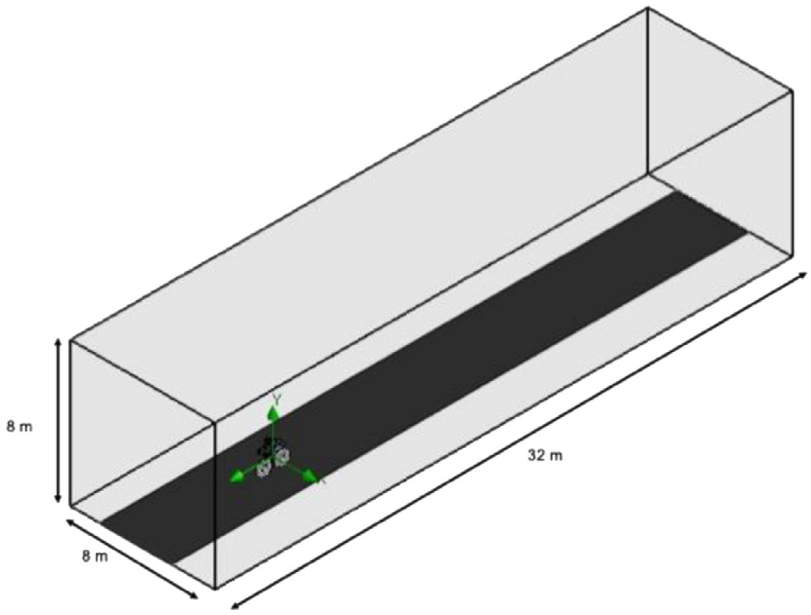

Fig. 2.5. Dimensions of the computational domain.

Table 2.1
Input and output parameters.

Input parameters and boundary conditions	Output parameters
• Inlet: air velocity	• Surface goal — Drag force
• Rotational velocity of bicycle wheels	• Equation goal — Drag coefficient
• Velocity of solid plane (no-slip moving wall)	• Surface goal — Lift force
• Cycle-cyclist assembly: no-slip wall	• Equation goal — Lift coefficient
• Outlet: ambient pressure	
• Left, right and top walls: slip wall	

order of 10^{-6}, as shown in Fig. 2.6. The results were tabulated post convergence and the next model was analyzed.

2.3. Grid independence study

In order to determine the grid size for the analysis, a grid independence study was performed. The values of drag coefficient were compared at various ratio factors at mesh level 7. The mesh level of the mesh quantifies the number of times the mesh has been refined, i.e. the maximum number of times the elements of the mesh have been divided in regions of greater complexity in geometry. A mesh level of 1 hence means a uniform mesh with elements of equal dimensions, while increasing refinement increases the fineness of the mesh. It may be noted from Fig. 2.10 that the Cartesian mesh is significantly finer in regions close to the model. The ratio factor of the mesh is the proportion between the aspect ratios of elements of consecutive levels of refinement. A high ratio factor hence leads to finer and better quality elements close to the model, and lower quality elements in regions farther away. This contributes to savings in computational time without compromising on accuracy. The study was conducted on the bicycle without cladding, at a velocity of 6 m/s with the k-ε model. It was observed that beyond a ratio factor of 8.5, the observed drag coefficient was minimally variant ($<1\%$), as evident from Fig. 2.7.

For further analysis of grid independence, 9 different line segments on the rotating region of the front bicycle wheel were analyzed. One-line segment passed through the center of the wheel and 4 each were present on either side of it, at equal intervals. Each line segment contained 11 points, geometrically distributed, as shown in Fig. 2.8. Grids of mesh level 7 and ratio factor 8.5, 9, 9.5 and 10 were studied. The number of cells in the meshes studied ranged from 4×10^6 to 5×10^6, with an average element characteristic length between 0.7 mm and 0.8 mm.

The velocity in the direction of travel (v) was plotted as a function of non-dimensional y-coordinate Y/Y_{max}, where the Y-coordinate of the point under consideration from the origin (assumed at the center of the wheel) is represented by Y and the maximum Y-coordinate for the line segment under study is represented by Y_{max}. All 4 meshes showed considerable mutual agreement. The results of two of the grid independence studies are shown in Fig. 2.9 for brevity. Trends of computational time are provided in Fig. 2.9; from which it is evident that an increase in ratio factor leads to a corresponding increase in computational time. Taking into account the results of the grid independence study, further analysis was carried out with a ratio factor of 8.5, using the mesh shown in Fig. 2.10.

3. Validation

The drag area (AC_D) values obtained from the study were considered for validation. Drag area is a coefficient introduced by (A brief introduction to fluid mechanics, 1997; Barratt, 1965; Pedley, 1997) as the ratio between the aerodynamic force and the dynamic pressure, and is considered useful in cases where the area of reference is not obvious, or the geometry consists of various parts (Zdravkovich, 1992). The drag area is regularly used as a parameter in both computational and experimental studies of bicycles (Blocken et al., 2013; Chowdhury et al., 2011a; Defraeye et al., 2010a; Zdravkovich, 1992).

The drag area values obtained through the current CFD analysis were validated against data reported by Zdravkovich et al. (1996) and Defraeye et al. (2010b). Zdravkovich et al. and Defraeye et al. conducted wind tunnel tests of bicycles in a similar

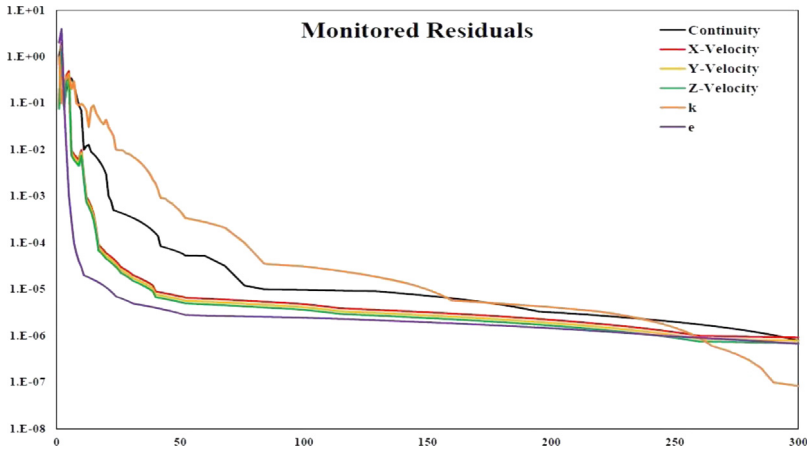

Fig. 2.6. Residuals for converged solution of bicycle without cladding at 6 m/s.

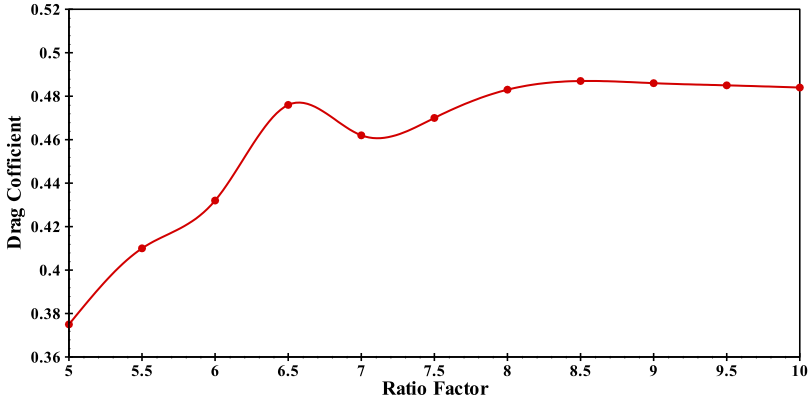

Fig. 2.7. Trend of drag coefficient with change in ratio factor.

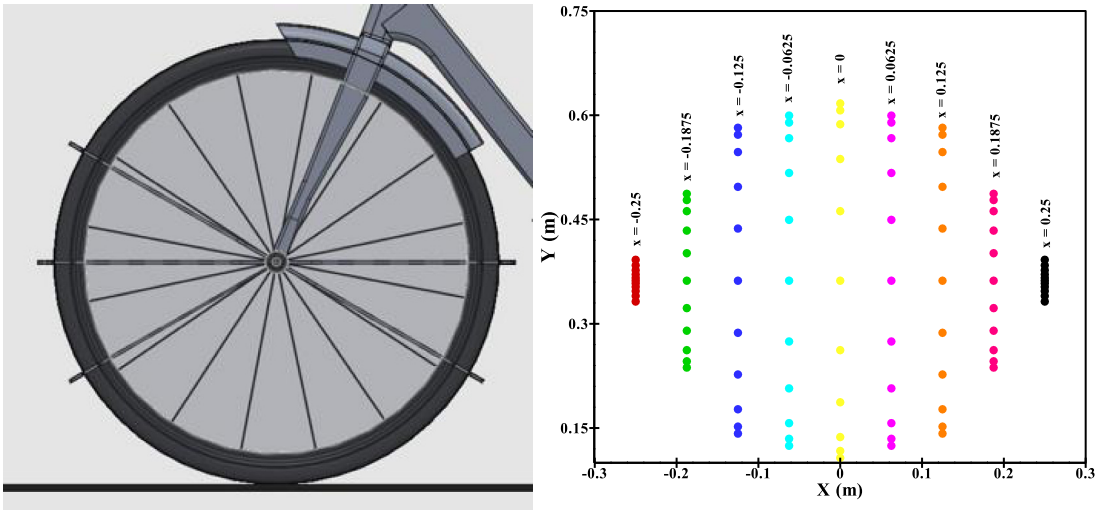

Fig. 2.8. (a) Region of CAD model studied for mesh independence (b) Cartesian coordinates of points analyzed for the mesh independence study.

context to the current study and at similar velocities. While Zdravkovich et al. obtained an average AC_D of 0.227, Defraeye et al. obtained a value of 0.243. The drag area values in the current study for the model with no cladding were found to be in agreement with experimental values of Zdravkovich et al. and Defraeye et al. obtained through their wind tunnel experiments. Table 3.1 summarizes the results.

4. Results and discussion

CFD analyses were conducted in order to predict drag force and drag coefficient as a function of percentage cladding on the

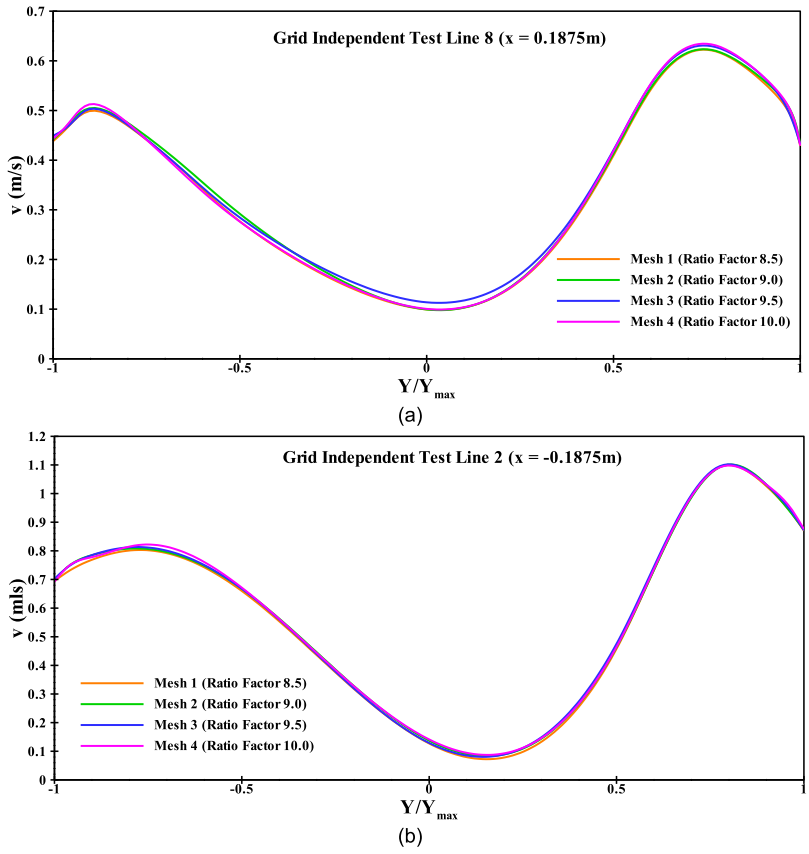

Fig. 2.9. Velocities for (a) Line 2 (b) Line 8 plotted against non-dimensional Y-coordinate at various ratio factors.

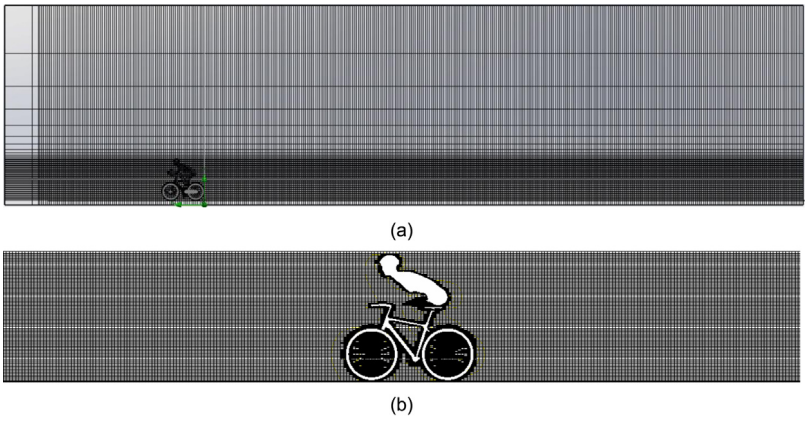

Fig. 2.10. Cartesian mesh used for analysis.

Table 3.1
Data reported in previous studies and obtained in current CFD analysis.

Study	AC_D (m^2)	Zdravkovich et al. AC_D (m^2)	Error (%)	Defraeye et al. (2010a) AC_D (m^2)	Error (%)
Current CFD Study, 10 m/s	0.237	0.227	4.40%	0.243	2.47%
Current CFD Study, 8 m/s	0.238	0.227	4.62%	0.243	1.64%
Current CFD Study, 6 m/s	0.238	0.227	4.81%	0.243	1.50%

wheels of a bicycle, for constant velocity, at velocities, 6 m/s, 8 m/s and 10 m/s. Fig. 4.1 depicts the velocity contours of the analysis conducted at a velocity of 10 m/s with 0% cladding. The drag experienced by the cyclist of primarily profile drag, which is created due to the presence of a pressure differential. The complex geometry of the cycle and cyclist makes the occurrence of adverse angles of attack for the air flow inevitable. This leads to adverse pressure gradients, which further cause separation of the flow from the body. This separation of flow leads to the development of a wake behind the cycle. It is observed that a considerable wake is generated behind the cyclist, which leads to the creation of vortices. In the region of the wake, significant losses in pressure take place due to eddy formation, which contributes to the creation of a low pressure region. This further increases the drag force experienced by the cycle and cyclist.

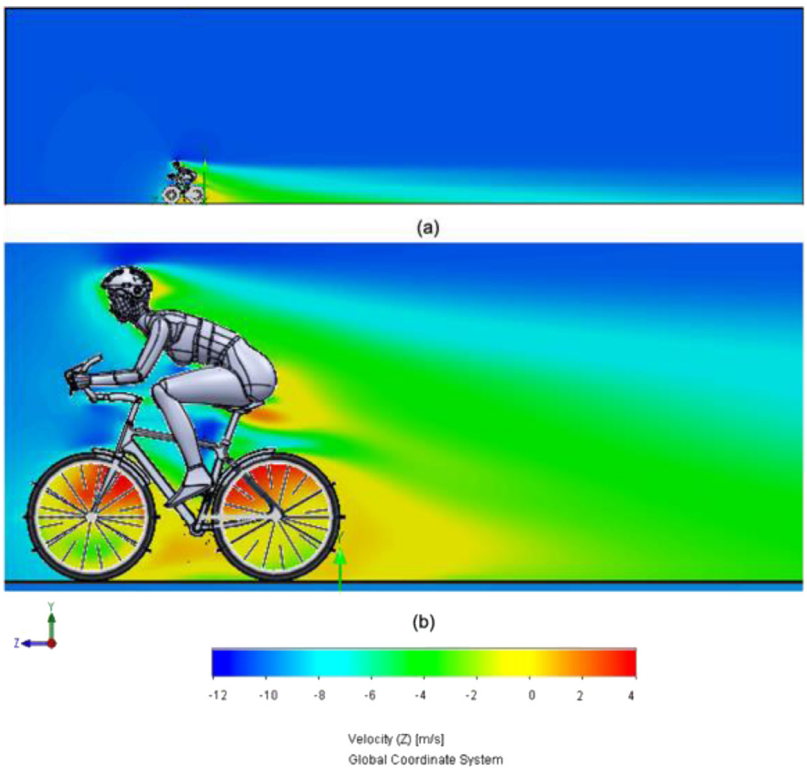

Fig. 4.1. Velocity contours of CFD analysis at air velocity of 10 m/s with 0% cladding (a) wide view (b) zoomed-in view.

Fig. 4.2 depicts the turbulence intensity in the region of the bicycle and rider at 0% and 100% cladding. It is evident from the figure that there is a marked difference between the turbulence intensities observed in the cycle with and without cladding, with the cycle with cladding possessing a considerably lower turbulence intensity in the region behind the wheels. This leads to a decrease in the low pressure region created at the wheel rear, leading to a decrease in the drag experienced by the cycle. In turbulent flows, a considerably large amount of energy is dissipated in the formation of eddies, leading to pressure losses. Hence, in comparison to laminar flow, turbulence has a greater contribution to drag. As turbulence increases, the region of low pressures exhibits greater efficacy in the development of drag force, which leads to an increase in drag.

Fig. 4.3 depicts the velocity streamlines for the analysis of the cycle at 5 m/s, with and without cladding. A significant reduction in turbulence, rotational velocity of air and irregularity of the vectors is observed in the cycle with cladding, alongside the presence of a smaller wake region. The presence of a cladding on the wheels of the bicycle provides the air with significantly lower exposure to adverse geometries such as wheels spokes, which exhibit a greater proclivity towards the separation of flow. Through this reduction in flow separation, the formation of eddies and regions of low pressure is also reduced. This leads to a reduction in turbulence and vorticity behind the wheels of the cycle, which lead to a reduction in the drag force.

Fig. 4.4 represents the drag force as a function of the percentage cladding on the bicycle wheels. From the graph, it is evident that the drag force shows a similar decreasing trend for all velocities under consideration. Fig. 4.5 represents the percentage change in drag force as compared to the model without cladding. All 3 velocities show a similar decrease for all models considered. This decrease is seen to proceed at a greater rate as the percentage increases. In experimental studies of a rotating cycle wheel conducted by Sayers and Stanley (1994), it was observed that wheels with cladding over the wheels exhibited

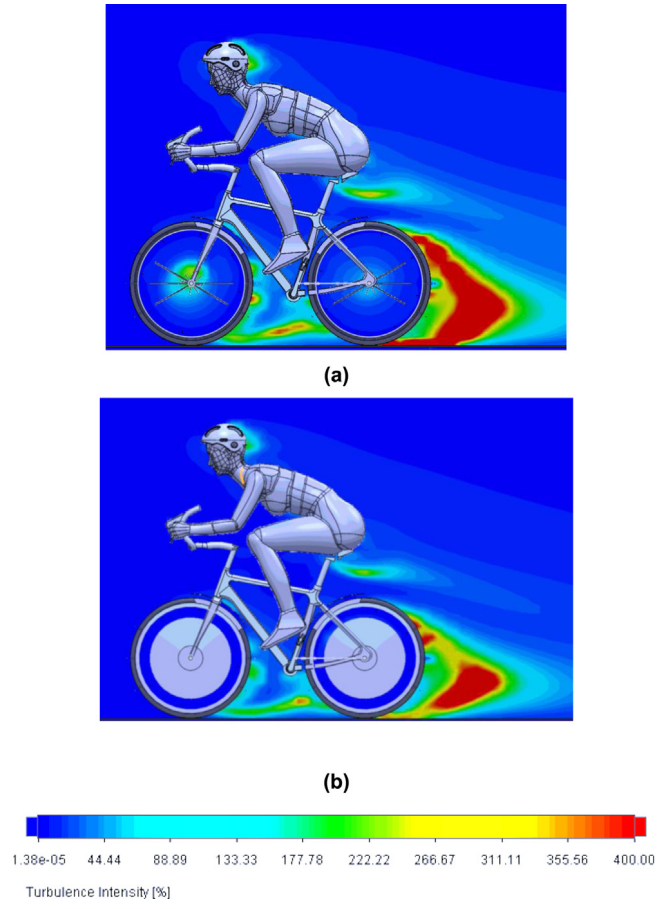

Fig. 4.2. Turbulence intensity contours for CFD analysis at (a) 0% cladding (b) 80% cladding.

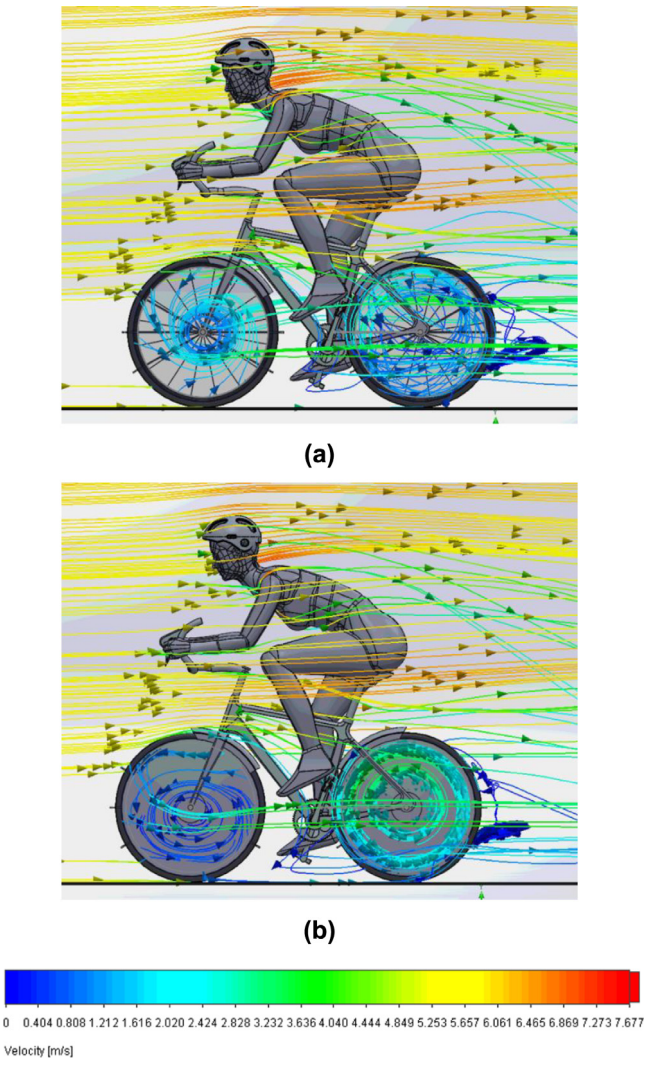

Fig. 4.3. Velocity streamlines at velocity 5 m/s with (a) 0% cladding (b) 100% cladding.

a considerably lower drag coefficient than wheels with spokes. This was attributed to the division of flow around the wheels. This division prevents the creation of eddies due to the rotation of the wheel, reducing drag. A change in velocity is found to have a negligible impact on the reduction in drag force.

Fig. 4.6 represents the drag coefficient as a function of cladding percentage at air velocities of 6 m/s, 8 m/s and 10 m/s. The drag coefficient at all 3 velocities shows similar trends of decrease. As in case of drag force, drag coefficient is observed to decrease steadily with increase in cladding. However, the rate of reduction increases with increasing percentage cladding. For any particular cladding percentage, the drag coefficient is found to increase with decrease in velocity. This follows research conducted by Grappe (2009) as reported by Debraux et al. (2011), where drag area (AC_D) was observed to decrease with increase in velocity, when velocities were within the range of the current study. Fig. 4.7 represents the percentage change in drag coefficient as compared to the model without cladding. As observed in case of drag force, the change in drag coefficient is similar in case of all 3 velocities. The minimum drag coefficient is observed at 100% cladding for all 3 velocities. The maximum reduction in drag coefficient is calculated as 5.3%, 5.3% and 5.2% for the 6 m/s, 8 m/s and 10 m/s case respectively.

The study conducted points toward the importance of a reduction in turbulence to improve the aerodynamics of a cycle. Introducing an accessory such as a cladding on the wheels of a bicycle can go a long way in reducing the aerodynamic drag of the bicycle, which is of much interest for both city and competitive cycling, as reduction in the drag produced by the cyclist can further lead to a reduction in the time taken to ride the same distance, as well as conservation of the energy consumed in doing so (Blocken et al., 2013; Swain, 1994).

In order to determine the physical effects of the change in drag force, the virtual gain in travel time is plotted as a function of cladding percentage in Fig. 4.8. This gain is calculated for a travel distance of 10 000 m at the velocities simulated. It is evident from the figure that the virtual travel time gained increases with increase in cladding percentage. The maximum gain varies from 23 s for a travel velocity of 10 m/s to 40 s for a velocity of 6 m/s. These gains are significant, especially considering that the decisions of competitive races hinge on margins of less than a second. It must however, be mentioned that these are only virtual gains; velocities during the race are often non-uniform, and factors such as drafting, track length and geometry and air flow can greatly change the actual times of travel.

5. Conclusion

- 3-dimensional CFD simulations were conducted using SolidWorks Flow Simulation in order to assess the impact of cladding on the aerodynamic drag force and drag coefficient of a cyclist riding a bicycle.

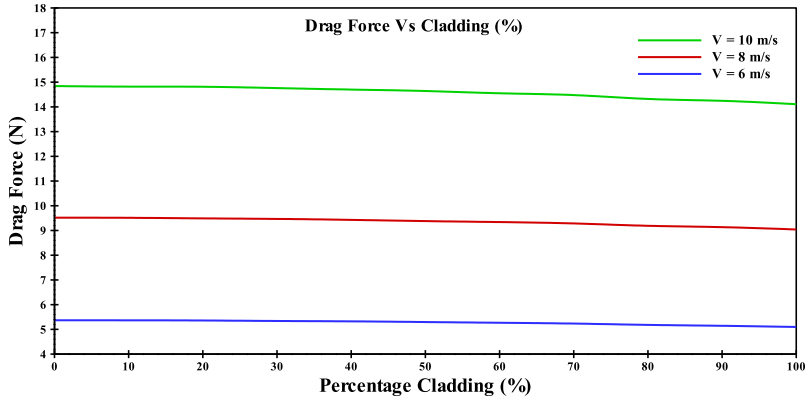

Fig. 4.4. Values of drag force experienced by bicycle-cyclist assembly at the analyzed velocities plotted against percentage cladding.

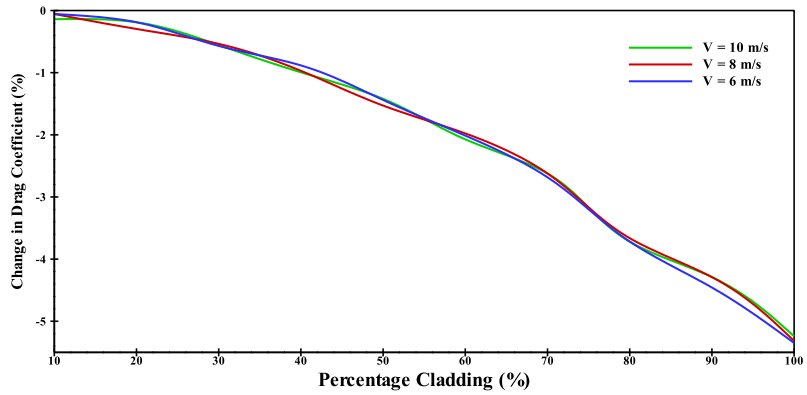

Fig. 4.5. Percentage change in drag force at the analyzed velocities plotted against percentage cladding.

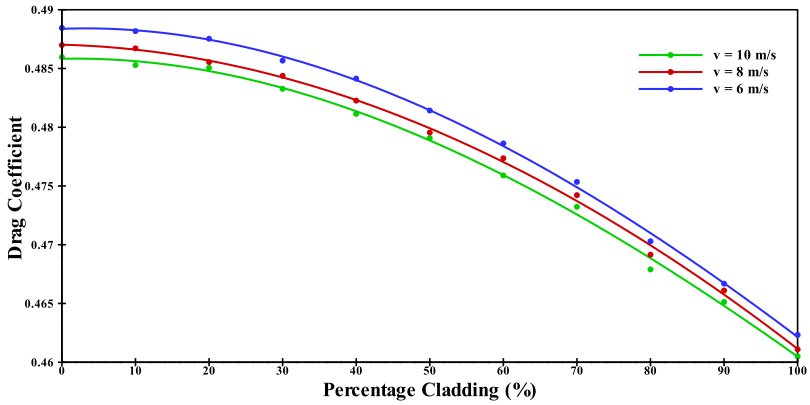

Fig. 4.6. Values of drag coefficient of the bicycle-cyclist assembly at the analyzed velocities plotted against percentage cladding.

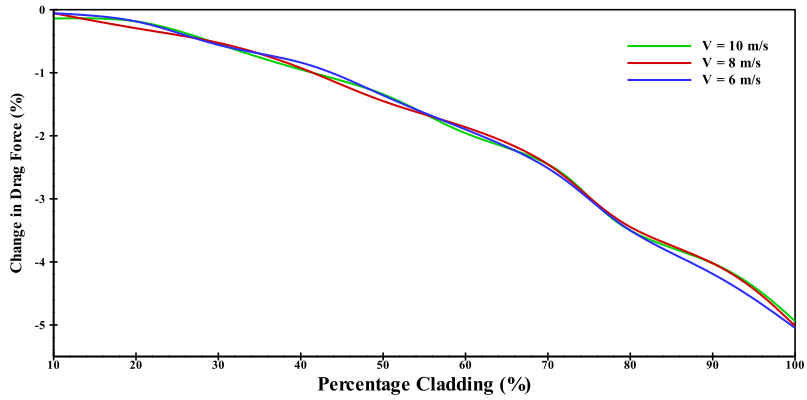

Fig. 4.7. Percentage change in drag coefficient at the analyzed velocities plotted against percentage cladding.

- Analyses were performed from a cladding percentage of 0% to 100% at velocities of 6 m/s, 8 m/s and 10 m/s, and the drag force and drag coefficient were seen to decrease with increase in cladding percentage. A maximum reduction in drag coefficient of 5.3%, 5.3% and 5.2% respectively in the 6 m/s, 8 m/s and 10 m/s case was computed.
- It is implied through all cases studied that the addition of cladding over the wheels of a bicycle is associated with a considerable change in drag force as well as drag coefficient. It is also observed that partial cladding of wheels has a lower effect on the drag coefficient than full cladding.
- While the increase in frontal area with addition of cladding is marginal, the aerodynamic impact is comparatively large.
- Drag force and drag coefficient both showcase a greater decrease in value for higher cladding percentages, while the decrease is marginal for lower cladding percentages. This reaffirms the positive aerodynamic impact of cladding on the wheels of a bicycle. A reduction in drag force and drag coefficient further implies a reduction in the effort required on part of the cyclist, as well as a reduction in time required to travel long distances.

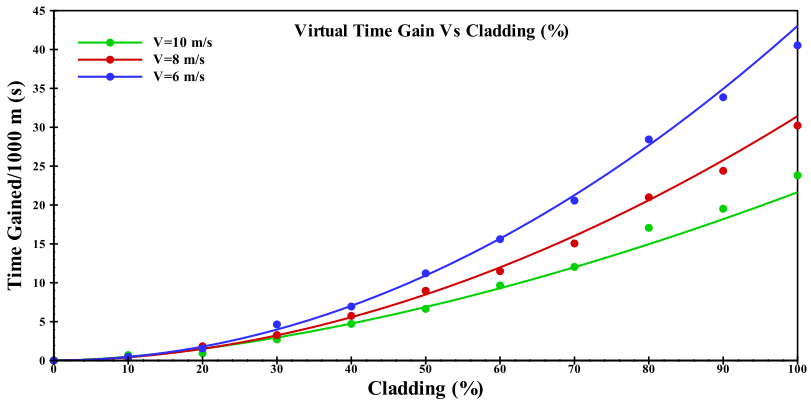

Fig. 4.8. Gain in travel time plotted against percentage cladding.

Nomenclature

ρ	Density of the medium	ε_e	Rate of dissipation of energy
t	Time	Q_H	Thermal energy
u_i	Velocity of flow in the x_i direction	C_D	Drag coefficient
u_j	Velocity of flow in the x_j direction	C_L	Lift coefficient
P	Fluid pressure	F_D	Drag force
τ_{ij}	Shear stress tensor	F_D	Lift force
S_i	Body force	A_D	Frontal area normal to the direction of travel
H	Total energy	A_L	Frontal area parallel to the road
h	Potential energy	v	Relative velocity of travel of the bicycle with respect to air
q_i	Heat flux in the x_i direction	ϕ	Diameter of cladding

Subscripts

i	x_i direction	L	Lift
j	x_j direction	D	Drag
e	Energy		

Superscript

R	Reverse tensor

Declaration of competing interest

The authors declare that they have no known competing financial interests or personal relationships that could have appeared to influence the work reported in this paper.

References

A brief introduction to fluid mechanics, 1997. Choice Rev. Online. http://dx.doi.org/10.5860/choice.34-5117.

Arora, B.B., 2014. Performance analysis of parallel hub diverging casing axial annular diffuser with 20° equivalent cone angle. Aust. J. Mech. Eng. http://dx.doi.org/10.7158/m11-823.2014.12.2.

Asadollahi, A., Rashidi, S., Esfahani, J.A., Ellahi, R., 2018. Simulating phase change during the droplet deformation and impact on a wet surface in a square microchannel: An application of oil drops collision. Eur. Phys. J. Plus http://dx.doi.org/10.1140/epjp/i2018-12135-6.

Barratt, M.J., 1965. The wave drag of a Hovercraft. J. Fluid Mech. http://dx.doi.org/10.1017/S0022112065000563.

Barry, N., Burton, D., Crouch, T., Sheridan, J., Luescher, R., 2012. Effect of crosswinds and wheel selection on the aerodynamic behavior of a cyclist. In: Procedia Engineering. http://dx.doi.org/10.1016/j.proeng.2012.04.005.

Blocken, B., Defraeye, T., Koninckx, E., Carmeliet, J., Hespel, P., 2013. CFD Simulations of the aerodynamic drag of two drafting cyclists. Comput. Fluids http://dx.doi.org/10.1016/j.compfluid.2012.11.012.

Chowdhury, H., Alam, F., Khan, I., 2011a. An experimental study of bicycle aerodynamics. Int. J. Mech. Mater. Eng..

Chowdhury, Harun, Alam, F., Mainwaring, D., 2011b. A full scale bicycle aerodynamics testing methodology. In: Procedia Engineering. http://dx.doi.org/10.1016/j.proeng.2011.05.057.

Crane, R., Morton, C., 2018. Drag and side force analysis on bicycle wheel-tire combinations. J. Fluids Eng. Trans. ASME http://dx.doi.org/10.1115/1.4039513.

Debraux, P., Grappe, F., Manolova, A.V., Bertucci, W., 2011. Aerodynamic drag in cycling: Methods of assessment. Sport. Biomech. http://dx.doi.org/10.1080/14763141.2011.592209.

Defraeye, T., Blocken, B., Koninckx, E., Hespel, P., Carmeliet, J., 2010a. Aerodynamic study of different cyclist positions: CFD analysis and full-scale wind-tunnel tests. J. Biomech. http://dx.doi.org/10.1016/j.jbiomech.2010.01.025.

Defraeye, T., Blocken, B., Koninckx, E., Hespel, P., Carmeliet, J., 2010b. Computational fluid dynamics analysis of cyclist aerodynamics: Performance of different turbulence-modelling and boundary-layer modelling approaches. J. Biomech. http://dx.doi.org/10.1016/j.jbiomech.2010.04.038.

Dyer, B.T.J., Noroozi, S., 2015. A proposed field test method and an assessment of the rotational drag of contemporary front bicycle wheels. Proc. Inst. Mech. Eng. Part P http://dx.doi.org/10.1177/1754337114545370.

Esfahani, J.A., Akbarzadeh, M., Rashidi, S., Rosen, M.A., Ellahi, R., 2017. Influences of wavy wall and nanoparticles on entropy generation over heat exchanger plat. Int. J. Heat Mass Transf http://dx.doi.org/10.1016/j.ijheatmasstransfer.2017.03.006.

Franke, J., Hellsten, A., Schlünzen, H., Carissimo, B., 2007. Best practice guideline for the CFD simulation of flows in the urban environment. COST Action.

García-López, J., Rodríguez-Marroyo, J.A., Juneau, C.E., Peleteiro, J., Martínez, A.C., Villa, J.G., 2008. Reference values and improvement of aerodynamic drag in professional cyclists. J. Sports Sci. http://dx.doi.org/10.1080/02640410701501697.

Godo, M.N., Corson, D., Legensky, S.M., 2009. An aerodynamic study of bicycle wheel performance using CFD. In: 47th AIAA Aerospace Sciences Meeting Including the New Horizons Forum and Aerospace Exposition. http://dx.doi.org/10.2514/6.2009-322.

Godo, M.N., Corson, D., Legensky, S.M., 2010. A comparative aerodynamic study of commercial bicycle wheels using CFD. In: 48th AIAA Aerospace Sciences Meeting Including the New Horizons Forum and Aerospace Exposition. http://dx.doi.org/10.2514/6.2010-1431.

Grappe, F., 2009. Reśistance totale qui s'oppose au deṕlacement en cyclisme [Total resistive forces opposed to the motion in cycling]. In: Cyclisme et Optimisation de la Performance, second ed. In: Cycling and optimisation of the performance, vol. 604.

Greenwell, D.I., Wood, N.J., Bridge, E.K.L., Addy, R.J., 1995. Aerodynamic characteristics of low-drag bicycle wheels. Aeronaut. J..

Hobeika, T., Sebben, S., 2018. CFD Investigation on wheel rotation modelling. J. Wind Eng. Ind. Aerodyn. http://dx.doi.org/10.1016/j.jweia.2018.01.005.

Ilea, L., Iozsa, D., Stan, C., Fratila, G., 2019. The impact of the wheel's rim on the aerodynamics of passenger vehicles. http://dx.doi.org/10.1007/978-3-319-94409-8_11.

Jermy, M., Moore, J., Bloomfield, M., 2008. Translational and rotational aerodynamic drag of composite construction bicycle wheels. Proc. Inst. Mech. Eng. Part P http://dx.doi.org/10.1243/17543371JSET17.

Jones, W.P., Launder, B.E., 1973. The prediction of laminarization with a two-equation model of turbulence. AIAA Sel. Represent. Ser. http://dx.doi.org/10.1016/0017-9310(72)90076-2.

Karabelas, S.J., Markatos, N.C., 2012. Aerodynamics of fixed and rotating spoked cycling wheels. J. Fluids Eng. Trans. ASME http://dx.doi.org/10.1115/1.4005691.

Kashyap, V., Bhattacharjee, S., 2019. Computational analysis of flap Camber and ground clearance in double-element inverted airfoils. In: SAE Technical Paper Series. http://dx.doi.org/10.4271/2019-01-5065.

Knupe, J., Farmer, D., 2009. Aerodynamics of high performance race bicycle wheels wing-light.de aerodynamics of high performance race bicycle wheels. Wing-light-de, Ger..

Kyle, C.R., Burke, E., 1984. Improving the racing bicycle. Mech. Eng..

Madhania, S., Muharam, Y., Winardi, S., Purwanto, W.W., 2019. Mechanism of molasses–water mixing behavior in bioethanol fermenter. experiments and CFD modeling. Energy Rep. http://dx.doi.org/10.1016/j.egyr.2019.04.008.

Mannion, P., Toparlar, Y., Blocken, B., Clifford, E., Andrianne, T., Hajdukiewicz, M., 2018. Analysis of crosswind aerodynamics for competitive hand-cycling. J. Wind Eng. Ind. Aerodyn. http://dx.doi.org/10.1016/j.jweia.2018.08.002.

Mansour, M.A., Bakier, M.A.Y., 2015. Influence of thermal boundary conditions on MHD natural convection in square enclosure using cu–water nanofluid. Energy Rep. http://dx.doi.org/10.1016/j.egyr.2015.03.005.

Milani Shirvan, K., Ellahi, R., Mamourian, M., Moghiman, M., 2017a. Effects of wavy surface characteristics on natural convection heat transfer in a cosine corrugated square cavity filled with nanofluid. Int. J. Heat Mass Transf http://dx.doi.org/10.1016/j.ijheatmasstransfer.2016.11.022.

Milani Shirvan, K., Mamourian, M., Mirzakhanlari, S., Ellahi, R., 2017b. Numerical investigation of heat exchanger effectiveness in a double pipe heat exchanger filled with nanofluid: A sensitivity analysis by response surface methodology. Powder Technol. http://dx.doi.org/10.1016/j.powtec.2017.02.065.

Monte, A.D., Leonardi, L.M., Menchinelli, C., Marini, C., 2016. A new bicycle design based on biomechanics and advanced technology. Int. J. Sport Biomech. http://dx.doi.org/10.1123/ijsb.3.3.287.

Pedley, T.J., 1997. Introduction to fluid dynamics. Sci. Mar. http://dx.doi.org/10.2307/j.ctvc77ddr.12.

Petrone, N., Giacomin, M., Koptyug, A., Bäckström, M., 2018. Racing wheels' effect on drag/side forces acting on a cyclist at sportstech-miun wind tunnel. In: Proceedings Vol. 2, p. 210. http://dx.doi.org/10.3390/proceedings2060210.

Pogni, M., Petrone, N., 2016. Comparison of the aerodynamic performance of five racing bicycle wheels by means of CFD Calculations. In: Procedia Engineering. http://dx.doi.org/10.1016/j.proeng.2016.06.192.

Rashidi, S., Akar, S., Bovand, M., Ellahi, R., 2018. Volume of fluid model to simulate the nanofluid flow and entropy generation in a single slope solar still. Renew. Energy http://dx.doi.org/10.1016/j.renene.2017.08.059.

Rashidi, S., Esfahani, J.A., Ellahi, R., 2017. Convective heat transfer and particle motion in an obstructed duct with two side by side obstacles by means of DPM model. Appl. Sci. http://dx.doi.org/10.3390/app7040431.

Sayers, A.T., Stanley, P., 1994. Drag force on rotating racing cycle wheels. J. Wind Eng. Ind. Aerodyn. http://dx.doi.org/10.1016/0167-6105(94)90094-9.

Schwab, A.L., Dialynas, G., Happee, R., 2018. Some Effects of Crosswind on the Lateral Dynamics of a Bicycle. In: Proceedings. http://dx.doi.org/10.3390/proceedings2060218.

Sobachkin, A., Dumnov, G., 2013. Numerical basis of CAD-embedded CFD. In: NAFEMS World Congress 2013.

Sunter, R.J., Sayers, A.T., 2001. Aerodynamic drag of mountain bike tyres. Sport. Eng. http://dx.doi.org/10.1046/j.1460-2687.2001.00070.x.

Swain, D.P., 1994. The influence of body mass in endurance bicycling. Med. Sci. Sports Exerc. http://dx.doi.org/10.1249/00005768-199401000-00011.

Tew, G.S., Sayers, A.T., 1999. Aerodynamics of yawed racing cycle wheels. J. Wind Eng. Ind. Aerodyn. http://dx.doi.org/10.1016/S0167-6105(99)00034-3.

Wickern, G., Zwicker, K., Pfadenhauer, M., 1997. Rotating wheels - their impact on wind tunnel test techniques and on vehicle drag results. In: SAE Technical Papers. http://dx.doi.org/10.4271/970133.

Yu, X., Jia, Q., Bao, D., Yang, Z., 2018. A comparative study of different wheel rotating simulation methods in automotive aerodynamics. In: SAE Technical Papers. http://dx.doi.org/10.4271/2018-01-0728.

Zdravkovich, M.M., 1992. Aerodynamics of bicycle wheel and frame. J. Wind Eng. Ind. Aerodyn. http://dx.doi.org/10.1016/0167-6105(92)90520-K.

Zdravkovich, M., Ashcroft, M.M., Chisholmet, S.J., Hicks, N., 1996. Effect of cyclist's posture and vicinity of another cyclist on aerodynamic drag. In: Haake, S. (Ed.), The Engineering of Sport, first ed..